7-1-2019

Synthesis and characterization of polylactide-PAMAM "Janus-type" linear-dendritic hybrids

Indika Chandrasiri
University of Mississippi

Daniel G. Abebe
University of Mississippi

Sudipta Gupta
Louisiana State University

Jon Steven Dal Williams
University of Mississippi

William D. Rieger
University of Mississippi

See next page for additional authors

Recommended Citation

Chandrasiri, I., Abebe, D., Gupta, S., Williams, J., Rieger, W., Simms, B., Yaddehige, M., Noh, Y., Payne, M., Fortenberry, A., Smith, A., Ilavsky, J., Grayson, S., Schneider, G., & Watkins, D. (2019). Synthesis and characterization of polylactide-PAMAM "Janus-type" linear-dendritic hybrids. *Journal of Polymer Science, Part A: Polymer Chemistry, 57* (13), 1448-1459. https://doi.org/10.1002/pola.29409

Watkins Davita (Orcid ID: 0000-0002-0943-7220)

/

Synthesis and Characterization of Polylactide-PAMAM "Janus-type" Linear-Dendritic Hybrids

Indika Chandrasiri,[a] Daniel G. Abebe,[a] Sudipta Gupta,[b] Jon Steven Dal Williams,[a] William D. Rieger,[a] Briana L. Simms,[a] Mahesh Loku Yaddehige,[a] YeRim Noh,[b] Molly E. Payne,[d] Alexander W. Fortenberry,[c] Adam E. Smith,[c] Jan Ilavsky,[e] Scott M. Grayson,[d] Gerald J. Schneider[b,f] and Davita L. Watkins[a*]

[a]Department of Chemistry and Biochemistry, University of Mississippi, University, Mississippi, 38677, United States
[b]Department of Chemistry, Louisiana State University, Baton Rouge, Louisiana 70803, United States
[c]Department of Chemical Engineering, University of Mississippi, University, Mississippi, 38677, United States
[d]Department of Chemistry, Tulane University, New Orleans, Louisiana 70118, United States
[e]X-ray Science Division, Argonne National Laboratory, 9700 South Cass Avenue, Lemont, Illinois 60439, United States
[f]Department of Physics & Astronomy, Louisiana State University, Baton Rouge, Louisiana 70803, United States
Correspondence to: Davita L. Watkins (E-mail: *dwatkins@olemiss.edu*)

Additional Supporting Information may be found in the online version of this article.

This is the author manuscript accepted for publication and has undergone full peer review but has not been through the copyediting, typesetting, pagination and proofreading process, which may lead to differences between this version and the Version of Record. Please cite this article as doi: 10.1002/pola.29409

ABSTRACT: Herein, we present a facile and comprehensive synthetic methodology for the preparation of polyester-PAMAM (i.e., polyester: polylactide, PLA (hydrophobic) and polyamidoamine, PAMAM (hydrophilic)) polymers. A library of PLA-PAMAM linear dendritic block copolymers (LDBCs) in which both L and D, L polylactide were employed in mass ratios of 30:70, 50:50, 70:30 and 90:10 (PLA:PAMAM) were synthesized and analyzed. When placed in aqueous media, the immiscibility of the hydrophilic and hydrophobic segments leads to nanophase-segregation exhibited as the formation of aggregates (e.g., vesicles, worms and/or micelles). By employing both stereochemical configurations of PLA, the differentiation in mass ratios of PLA-PAMAM aided in elucidating the structure-property relationships of the LDBC system and provided a means towards control of nanoparticle morphology. Transmission electron microscopy (TEM) and dynamic light scattering (DLS) afford the size and shape of the nanoparticles with diameters ranging from 10.6 for low mass ratios to 122.4 nm for high mass ratios of PLA-PAMAM and positive zeta-potential values between +24.7 mV to +48.2 mV. Furthermore, small-angle X-ray scattering (SAXS) studies were employed to obtain more detailed information on the morphological assemblies constructed via direct dissolution. Such insights provide a pathway towards nanomaterials with unique morphologies and tunable properties deemed relevant in the development of next generation biomaterials.

KEYWORDS: linear dendritic block copolymers, amphiphilic polymers, polylactide, polyamidoamine,

INTRODUCTION

Synthetic polymers such as dendrimers and linear block copolymers have been studied extensively in the development of drug delivery systems (DDS) due to the complex macromolecular structures obtained by tailored and differentiated monomer compositions.[1-3] Among these multifaceted polymeric constructs are applications of amphiphilic or "Janus-type" linear-dendritic block copolymers (LDBCs).[4] Often referred to as hybrid materials, Fréchet et. al, introduced the concept of LDBCs in the early 90s, where a linear polymer is conjugated to a dendritic unit in a range of different configurations.[5] By combining the advantageous properties of both linear and dendritic (i.e., branched) macromolecules, these polymers result in a composition of segments with different molecular architectures and chemical properties. An interesting property exhibited by these polymers is the formation of various types of supramolecular aggregates in water, depending on the mass ratio between the hydrophilic and hydrophobic moieties.[6] In contrast to traditional polymers, the nanostructures formed from linear–dendritic macromolecules possess superior mechanical properties as well as high degrees of molecular uniformity.[7] However, lack of synthetic feasibility has hindered the widespread adoption of amphiphilic LDBCs due to challenges with distinct solubility of the blocks, steric effects of the branched block on copolymerization and purification of end products.[8, 9] In addition to these difficulties, the traditional mass ratio heuristic used with linear polymers does not accurately support these nonlinear, anisotropic systems.[10]

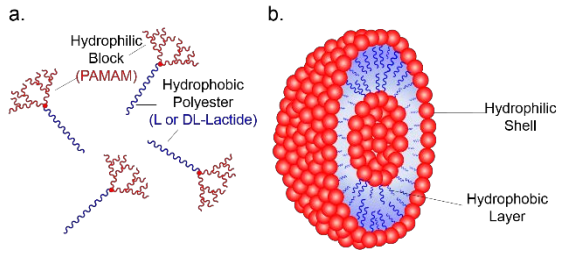

Figure 1. Graphical illustration of (a) Janus type (linear-dendritic block copolymers) LDBCs made of polyamidoamine (PAMAM) and polylactide and (b) expected bilayered vesicles formed in water by the LDBCs

Considering the components that constitute the molecular framework of LDBCs and contribute to the properties of the resulting nanostructure, a diverse range of building units can be investigated for further applications. Of particular interest is that of polyamidoamine (PAMAM) and polyesters. PAMAM is a hydrophilic dendrimer comprised of an amide backbone. Its structural cavities afford opportunities for encapsulation of small molecules via noncovalent interactions,[11, 12] mainly hydrogen bonding. The terminal free amine groups provide a positive-charge surface density suitable for biological applications (i.e., cell binding and endocytosis).[13, 14] Naturally, PAMAM has found wide interest as a drug delivery vector and there is a large body of established work in terms of its drug encapsulation, transfection efficiency and delivery capacity.[15]

In a review of the type of linear polymers utilized in LDBCs, a limited few have been reported—those of which include poly(ethylene oxide), poly(2-methyl-2-oxazoline), poly(styrene), and poly(propylene oxide).[4] Most notable are those LDBCs created with the biodegradable biocompatible polyester, polylactide (PLA). PLA is one of the few hydrophobic polymers that can have its stereochemical structure modified by polymerizing the D or L form of the monomer.[16] It is also one of the most well characterized and widely applied polymers for biomedical applications.

In regards to the applications of these unique polymers, the number of published articles in which PAMAM and polyesters have been combined as linear diblock copolymers are few in number.[17-20] Qiao et al. synthesized PAMAM-PLLA LDBCs by ring-opening polymerization (ROP) of D,L-lactide using stannous octoate ($Sn(Oct)_2$) with a half-generation PAMAM dendron as the macro-initiator.[21] The micellar nanoparticles prepared in their study, however, faced stability challenges and stable nanoparticles (NPs) could only be prepared at high PAMAM weight ratios.[21] Although the study generated promising materials for potential biomedical application, the design and methodology lacked in the synthetic versatility that is needed to yield high performing materials.

We have undertaken a systemically different approach to explore the potentials of merging PAMAM and polyesters into a single polymer. Herein, we present a facile and comprehensive synthetic methodology for the preparation of polyester-PAMAM (i.e., polyester: polylactide, PLA (hydrophobic) and PAMAM (hydrophilic)) polymers. Aspiring to develop next generation drug delivery systems (DDS) (Fig.1), it is our belief that the combination of these polymers—which each have individually long pedigrees in material science—can lead to the establishment of unique materials through compositional and architectural control. A library of 30, 50, 70, and 90 (i.e., weight percentage with respect to PLA) LDBCs of both L and DL were synthesized and analyzed using nuclear magnetic resonance (NMR), gel permeation chromatography (GPC), thermogravimetric analysis (TGA) and differential scanning

calorimetry (DSC). Different mass ratios of PLA-PAMAM using both stereochemical configurations of PLA were synthesized in order to elucidate the structure-property relationships (i.e., resulting structure in respect of polyester type and mass ratio) of the LDBC system; thus, facilitating control of nanoparticle size and shape. Nanoparticles were then formed in aqueous media, and the resulting structures were studied by dynamic light scattering (DLS), transmission electron microscopy (TEM), and small-angle X-ray scattering (SAXS).

EXPERIMENTAL

Materials and Methods

Reagents and solvents were purchased from commercial sources and used without further purification unless otherwise specified. Tetrahydrofuran (THF) and dimethylformamide (DMF) were degassed in 20 L drums and passed through two sequential purification columns (activated alumina; molecular sieves for DMF) under a positive argon atmosphere. All synthetic procedures were carried out under argon atmosphere using standard Schlenk line techniques unless otherwise stated. 1,8-diazabicyclo[5.4.0]undec-7-ene (DBU) (98 %, Acros) and chloroform (99.9 %, Acros) were distilled over CaH_2. All lactide monomers (L, DL) were recrystallized using toluene and dried under high vacuum (-100 kPa). Macroinitiator (**HO-G3Boc**) used for ROP was freeze dried before use. All the weighing for ROP was done in a glove box. Additional synthetic details, general procedures and tabulations of materials characterization can be found in the electronic supporting information (ESI†).

General Synthesis

The copolymers were synthesized using a "dendrimer first" approach[22] in which the dendritic segment acts as an initiator for ROP of the linear segment (Scheme 1). Briefly, the PAMAM dendron was synthesized by a divergent method in which the growth of the dendron was originated from a core functional group. Using ethanolamine as the focal point, a Michael addition with methyl acrylate formed a half-generation dendron, followed by nucleophilic amidation with ethylenediamine to afford full generation dendrimers. This was repeated up to generation 3 (G3). The amine-terminated dendron was treated with di-*tert*-butyl dicarbonate in methanol to obtain **HO-G3Boc** in 90 % yield (Scheme S1.). The Janus-type LDBC intermediates (i.e., precursors **L-G3Boc** and **DL-G3Boc**) were prepared by ROP of L-lactide or D,L-lactide employing DBU as the catalyst. Variations in monomer feed gave the precursors in weight ratios of 90, 70, 50, and 30 % with respect to PLA. The percentages indicate the weight ratio of the hydrophobic block with respect to the total weight of the amphiphilic block copolymer. For example, if the system is 90 %, the hydrophobic polyester block contains the 90 % of mass of the block copolymer.

Removal of the Boc protecting group using trifluoroacetic acid (TFA) afforded the final LDBC products **L-G3** and **DL-G3**. Additional information regarding molecular weight calculations and nomenclature for the resulting copolymers as well as a detailed synthetic procedure are presented in the ESI†.

Characterization of Boc-protected Intermediates

^{1}H NMR spectra of PAMAM dendrons and Boc protected precursors were performed on a Bruker Avance spectrometer (Bruker, Germany), operating at 500 MHz with $CDCl_3$ or MeOD-d_4 as the solvent and TMS as an internal standard. The degree of polymerization of PLA was estimated by the integration values of the peaks

corresponding to methylene protons as well as Boc protons using ^{1}H NMR. Molecular weight and PDI of the copolymers were determined by gel permeation chromatography (GPC). All the measurements were done using either DMF or THF. THF measurements were done at a flow rate of 1 mL/min at 35 °C. A Shimadzu 20A GPC system equipped with two Jordi Gel DVB500 columns and a differential refractive index detector was used. Polystyrene standards (900–100,000 g/mol) were used for the calibrations curve and the data were processed using a LCSolution ver.1.21 GPC option software. DMF measurements were done at flow rate of 0.3 mL/min at 50 °C, on a GPC system equipped with Waters Alliance HPLC System, 2695 Separation Module with 2 Tosoh TSKgel Super HM-M columns and Waters 2414 Differential Refractometer (RI) and Waters 2998 Photodiode Array Detector (PDA) was used. Polystyrene standards (900–100,000 g/mol) were used for the calibrations curve and data were processed using Empower 3 software (Waters). An addition of the electrolytic salt, LiBr (0.01%) was done to minimize effects such as polymer aggregation and/or adsorption associated with the polymer or the columns, enabling normal fractionation to occur.[23-25]

Matrix-assisted laser desorption time of flight mass spectrometry (MALDI-TOF MS) data was acquired using a Bruker-Daltonics Autoflex III mass spectrometer with delayed extraction using the reflector and positive ion mode. The samples were prepared by combination of polymer analyte (2 mg/mL) in THF, *trans*-2-[3-(4-tert-butylphenyl)-2-methyl-2-propenylidene] malononitrile (DCTB) (20 mg/mL) in THF as the matrix, and sodium trifluoroacetate (2 mg/mL) in THF as the counter ion in a 15:15:1 ratio. MALDI-TOF MS data were calibrated against SpheriCal dendritic calibrates from Polymer Factory (Stockholm, Sweden). M_n and M_w for all polymers were calculated using PolyTools software. Additional results of characterization are presented in the ESI.

Preparation and Characterization of Self-assembled Aggregates

Thermal analysis of the LDBCs was conducted using thermogravimetric analysis (TGA) and differential scanning calorimetry (DSC). TGA measurements were performed on Seiko Instruments TG/DTA 6200 (platinum pan, room temperature to 600 ^{o}C, ramp rate of 20 ^{o}C min^{-1} under nitrogen atmosphere) and analyzed with MUSE Analysis software. DSC scans were performed on TA Instruments DSCQ1000-0620 v9.9 (sealed aluminium pan, empty aluminium reference pan, ramp rate of 20 ^{o}C min^{-1}, two heating and cooling cycles) and analyzed on Universal Analysis 2000 4.4A software.

The LDBCs having weight ratios of 70:30, 50:50, and 30:70 (in respect to PLA) were formed into aggregates employing a direct dissolution method.[26-28] Aggregates for LDBCs with ratios of 90:10 were formed using nanoprecipitation.[27, 29] For direct dissolution, 1 mg of LDBC was added to a vial of MilliQ water (1 mL) while stirring followed by sonication to achieve homogeneity. The nanoparticle suspension were allowed to stabilize at room temperature for 12 hours. Nanoparticles formed via the nanoprecipitation method used acetone or THF (according to the solubility properties of the each system) as the organic solvent to dissolve 1 mg of LDBC in a glass vial. The solution was added dropwise to a separate vial of MilliQ water (1 mL) while stirring and sonication followed thereafter. Acetone/THF was allowed to evaporate under a stream of nitrogen. Nanoparticles solutions were allowed to equilibrate for 12 hours before testing.

Aggregate size and zeta potentials (ζ-potential) were determined by dynamic light scattering (DLS). Measurements were carried out on a Malvern Instrument

Zetasizer Nano ZS using a He–Ne laser with a 633 nm wavelength, a detector angle of 173° at 25 °C using a He–Ne laser with a 633 nm wavelength. The vesicle concentration was 1 mg mL^{-1} and size measurements were performed three times on each sample to ensure consistency. The morphological study of the aggregates formed from the LDBCs was carried out by transmission electron microscopy (TEM) using a JEOL 1230 TEM was operated at 100 kV to collect the transmission electron microscopy images using a Gatan Orius 831 bottom mounted CCD camera.

For critical aggregation concentration (CAC) measurements, pyrene (1.7 mg, 8.41 µmol) was dissolved in 3.34 mL of acetone and 40 µL of the solution was added to 39.96 mL of deionized water. A series of twelve concentrations of the nanoparticle suspension ranging from 10^{-8} mg L^{-1} to 1000 mg L^{-1} was prepared by dilutions of 1.8 mL per sample. A 1.8 mL of the pyrene solution was added to each vial, and these solutions were equilibrated for 48 hours in the absence of direct light. The fluorescence spectra were obtained on a Varian Cary fluorescence spectrometer from Agilent Technologies. An emission wavelength of 390 nm was used for pyrene and the excitation spectra were recorded from 300 to 360 nm. The ratio of emission intensities at 338 and 333 nm was graphed as a function of the log of the concentration. The CAC was determined as the concentration at the intercept of the lines for the two linear regions of the obtained graphs (ESI).

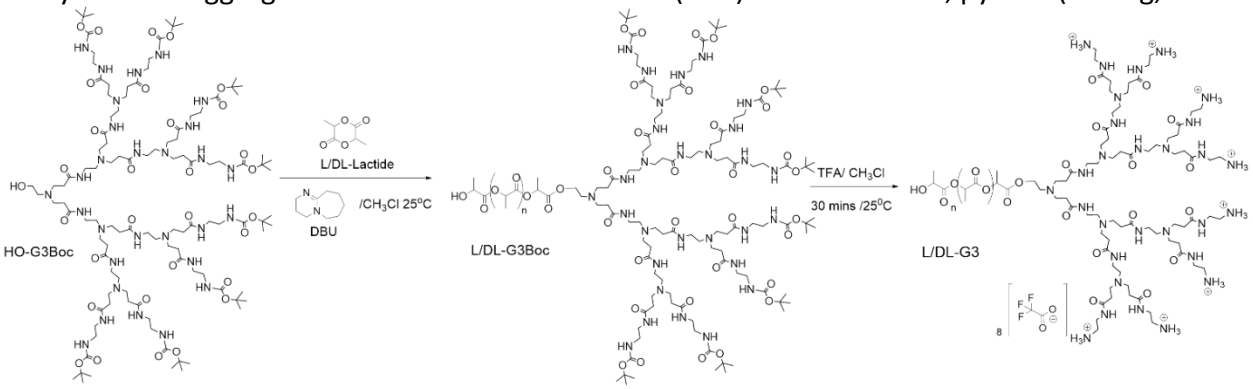

Scheme 1. Synthetic route for LDBCs by ring opening polymerization of lactide initiated by **HO-G3Boc** macroinitiator

Small angle X-ray scattering (SAXS) was performed at the Advanced Photon Source at 9-ID-C beamline, operated by the X-ray Science Division. It covers a range in momentum transfer Q, from 0.002 to 0.5 $Å^{-1}$, where $Q = 4\pi\sin(\vartheta)/\lambda$, for the scattering angle ϑ and X-ray wavelength λ = 0.59Å at energy 21 keV. All data reduction into intensity $I(Q)$ or, the macroscopic scattering cross-section $d\Sigma/d\Omega$ vs. momentum transfer $Q = |\vec{Q}|$ was carried out following the standard procedures that are implemented in the Nika software package.[30] The solvent was subtracted as the background by measuring water separately.

RESULTS AND DISCUSSION

Design and Synthesis of Polyester-PAMAM LDBCs

An illustration of the PLA-PAMAM LDBCs of study are shown in Figure 1a. The hydrophilic block which consists of dendritic

PAMAM was chosen due to its synthetic accessibility allowing a variety of functional groups to be readily incorporated. Possessing a hyperbranched polymeric structure, the backbone of PAMAM mimics the polypeptide nature of many biological species present in the body.[15] Such a structure renders the PAMAM portion more biocompatible than other traditional dendrimeric systems.

Opposite is the hydrophobic polyester block, either PLLA (L) or PDLLA (DL). These hydrophobic polymer chains drive the self-assembly of the nanostructures. These were systematically chosen for two purposes: (1) extended pedigree as biocompatible and biodegradable biomaterials and (2) accessible range of thermal and mechanical properties (i.e. crystalline vs amorphous).[16] By utilizing the 1:1 mixture of D and L-lactide monomer, the heterotactic PDLLA is achieved. This polymer is amorphous and does not exhibit a melting temperature (T_m). Alternatively, the pure L-lactide monomer yields the isotactic PLLA which is semi-crystalline possessing a T_m above 180 degrees.[31] The differences between crystalline PLLA and amorphous PDLLA provided an opportunity to probe the effects

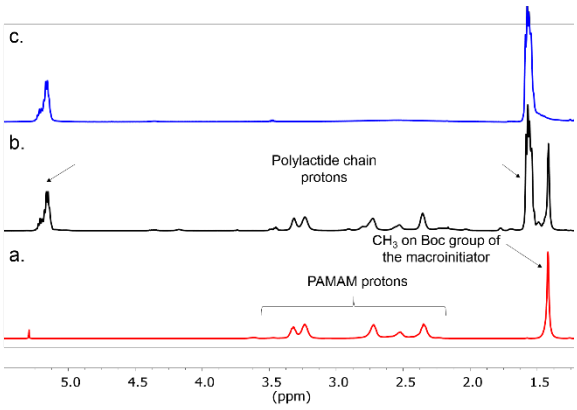

Figure 2. NMR comparison of the (a) macroinitiator **HO-G3Boc**, (b) LDBC precursor **70-DL-G3-Boc** and (c) amphiphilic LDBC **70-DL-G3** as a reverse micelle. Peaks from 2.19 ppm to 3.69 ppm refer to the protons signals for PAMAM-G3-Boc (Figure S7, SI sample 8). The resonance peaks corresponding to the primary and tertiary hydrogens on the liner polylactide chain appear at 1.57 and 5.15 ppm (Figure S9, SI LDBC samples 9 and 10).

of monomer composition on the morphology and thermodynamic properties of the resulting self-assembled nanostructure.

The general synthesis of **L-G3** and **DL-G3** is depicted in Scheme 1. Boc protected PAMAM (G3) possessing a hydroxyl focal-point was synthesized in five steps (Scheme S1) and used as the macroinitiator (**HO-G3Boc**) for ROP of either L- or DL-lactide monomer to yield LDBC precursors, **L-G3Boc** and **DL-G3Boc** in mass ratios of 90:10, 70:30, 50:50
and 30:70 PLA to PAMAM. Under mild conditions, the Boc protecting group is readily removed using TFA to yield the target LDBCs, **L-G3** and **DL-G3**. While others have been limited to <50 weight % hydrophobic content in order to form stable aqueous nanoparticles,[21] the amine protection/de-protection approach utilized here allowed us to prepare copolymers containing up to 90 weight % hydrophobic polymer while still possessing enough hydrophilic character to self-assemble into stable nanostructures in aqueous solution.

In employing a dendrimer first approach, characterization of the macroinitator, **HO-G3Boc**, is critical. The Boc group was installed to prevent ROP off of the terminal amines and additional side reactions at the periphery of the PAMAM dendron. MALDI-TOF mass spectrometry was used to validate the structural integrity of the PAMAM dendron and reactivity of the hydroxyl focal-point as steric inhibition has been a reported challenge for the synthesis of LDBCs.[32, 33] For the latter, **HO-G3Boc**

exhibiting a mass to charge ratio of 2481 m/z $[M+Na]^+$ was treated with acetic anhydride (Fig. S12). The product was purified and analyzed via mass spectrometry to reveal a difference in mass of 42 m/z corresponding to the addition of an acyl group at the focal-point and sole reactivity of the hydroxyl group on **HO-G3Boc** (Fig. S13)**.**

Verification by both ^{1}H NMR spectroscopy (Fig. 2a) and mass spectrometry (Fig. S14) supported further use of **HO-G3Boc** in ROP of L- and DL-lactide. Reactions were conducted with DBU as the catalyst in anhydrous chloroform and purified via precipitation in a mixture of diethyl-ether, hexane and methanol (15:5:1). It is imperative to note that the ROP step was optimized for DBU as the catalyst, rather than the traditional $Sn(Oct)_2$.[34] During synthesis development, the concentration of $Sn(Oct)_2$ required to achieve >90% monomer conversion was much higher, particularly at higher PAMAM weight ratios, than the 5% (per hydroxyl initiator) previously reported.[21] We observed a mere 8% monomer conversion for our copolymers with 5% catalyst loading and required ~20% $Sn(Oct)_2$ to reach monomer conversion >90%. When the polyester weight ratio is higher, e.g. 70:30, slightly less $Sn(Oct)_2$ is required (~15%) to drive lactide monomer conversion to > 90% . Rationale for such high loading of $Sn(Oct)_2$ are not fully understood, however, it is feasible to assume catalyst deactivation or sequestration through interactions with the PAMAM macroinitiator is the cause. Polymerization kinetic studies are actively on-going with the focus on understanding initiation, propagation and competing events such as depolymerization and catalyst deactivation.

Because the higher loading of a potentially toxic metal catalyst is counter-productive to the biomedical-driven application of the study, a number of other organometallic (zinc undecylenate) and organic (4-dimethylaminopyridine, DBU, triazabicyclodecene) catalyst systems previously reported for ROP of lactides were screened (Table S1).[35-38] DBU was found to be the most efficient catalyst, leading to near quantitative monomer conversion at all weight ratios investigated. In addition, the use of DBU afforded further advantages, such as reduced reaction time (4 hour), mild reaction conditions (25°C), and quantitative removal of the resulting DBU-benzoate salt which eliminates the presence of residual cytotoxic catalyst within the polymer.

As shown in Figure 2, an overlay of NMR spectra shows characteristic peaks of PAMAM (2.19 - 3.69 ppm) and polylactide (1.57, 5.15 ppm). Both segments are present in the spectrum of the coupled product for precursor **70-DL-G3-Boc** where 70 denotes the percentage of DL-lactide composing the LDBCs (Fig. 2b). Boc-protected LDBCs show high solubility in common solvents such as chloroform and THF; however, upon deprotection of the PAMAM block with TFA to yield **70-DL-G3**, solubility dramatically decreased due to the formation of NH_3^+ terminal groups (Scheme 1). NMR spectra of deprotected **70-DL-G3** (Fig. 2c; chloroform-*d*) give indirect evidence of solvent-driven aggregation by the disappearance of resonance peaks for PAMAM, while polylactide peaks remain visible. No precipitation is observed in the chloroform-*d* solution, which suggests the formation of a reverse-micelle where PAMAM is shielded from the solvent (i.e, micelle core) and PDLLA acts as a stabilized shell. Such analyses have been reported by others to give indirect confirmation of a covalently linked copolymer with both hydrophilic and hydrophobic components.[39]

Molecular Weight Analysis of LDBCs

Aiming to correlate feed ratios to that of molecular weight and degree of polymerization, further characterization of

the products was required. The precursors were studied due to the limited solubility of the deprotected LBDCs and tabulation of the results are given in Tables 1 and S2-3 and molecular weight calculations are given in Table S3. Initially, MALDI and GPC presented a unique challenge for these systems. In the case of MALDI, ionization of the PAMAM species only occurred in a small subset of solvent/matrix combinations that were tested. Such challenges have been noted in the literature.[40-43] In contrast, GPC gave better results particularly for precursors with a greater mass percentage of polylactide (i.e., **90-DL-G3Boc**, **70-DL-G3Boc**, **90-L-G3Boc** and **70-L-G3Boc**). As the calibration curve was created with a linear polystyrene standard, the hydrodynamic volume of these polymers did not correlate perfectly, as dendrons are more compact. For LDBCs with a greater linear (i.e., polylactide) portion, the peaks displayed a more Gaussian nature, whereas in systems that had a higher weight percentage dendritic portion (i.e., **50-DL-G3Boc**, **30-DL-G3Boc**, **50-L-G3Boc** and **30-L-G3Boc**), there was a deviation from the normal distribution, with shoulders appearing adjacent to the major peak (Fig. S16, S17). Upon changing the solvent from THF to DMF, an improved chromatographic behavior is seen presumably due to increased solubility of LDBCs with higher PAMAM ratios in the more polar solvent (ESI).

Table 1. Molecular weight characterization of PLA-PAMAM LDBCs of varying weight ratios by GPC with DMF as the elution solvent; chromatographs shown in Figure S14-15

LDBCs[a]	M_{th} g mol^{-1}	M_n g mol^{-1}	M_w g mol^{-1}	Đ
90-L-G3Boc	17,465	12,084	20,659	1.71
70-L-G3Boc	6350	8,189	12,012	1.52
50-L-G3Boc	4127	5,205	6,565	1.28
30-L-G3Boc	3175	3,862	4,248	1.10
90-DL-G3Boc	17,465	15,303	24,203	1.58
70-DL-G3Boc	6350	8,255	11,688	1.47
50-DL-G3Boc	4127	5,540	6,972	1.28
30-DL-G3Boc	3175	4,402	4,941	1.13

[a]Notation of **L-G3** and **DL-G3** denotes LDBC composition where L: PLLA or DL: PDLLA linked to a G3 PAMAM with weight percentage of lactone attributed and M_{th} , Mn, Mw, Đ denote theoretical molar mass, number average molar mass, weight average molar mass and dispersity respectively.

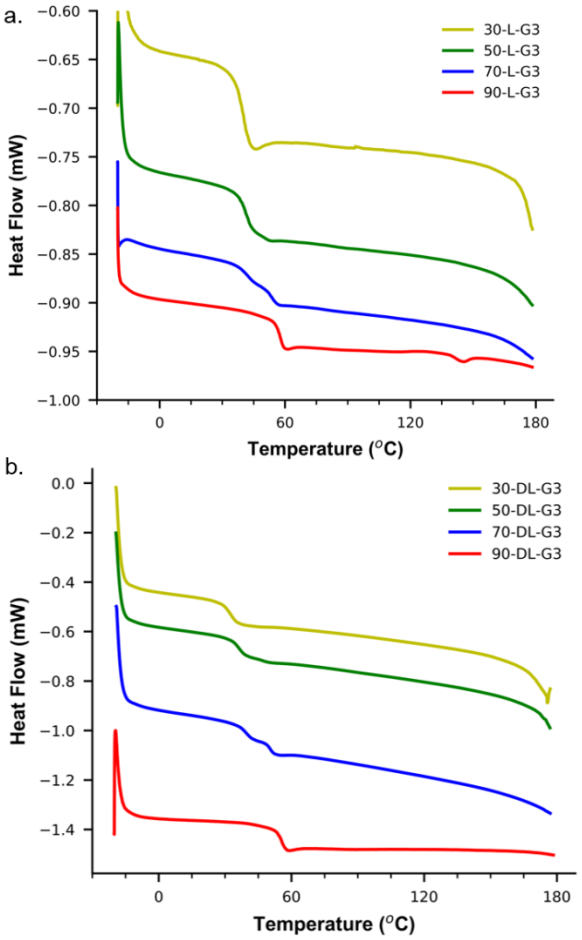

Figure 3. DSC traces of (a) L-G3 and (b) DL-G3 LDBCs under heating at 20 °C min^{-1} under a nitrogen atmosphere

Thermal Analysis

Thermal analysis via TGA (Fig. S18) and DSC (Fig. 3) was achieved using deprotected LDBCs. In this case, all polymers have NH_3^+ end groups, unless otherwise noted. The amine end groups are expected to have some effect on thermal stability due to the possibility of intramolecular hydrolysis or hydrogen bonding. DSC was done up to 180 °C in all cases, which is approximately the onset of decomposition according to TGA. Unfortunately, T_ms were not attainable for **L-G3**.

Thermal stability followed the general trend of increasing as the total molecular weight increased (Table S2). LDBC **90-L-G3** exhibits a higher decomposition temperature than that of **90-DL-G3** presumable due to it crystalline nature.[44, 45] The one exception was **30-L-G3**, which displayed an increase in thermal stability versus **50-L-G3**. All **L-G3** LDBCs except **90-L-G3** showed a slight decrease in thermal stability before the decomposition point, which is hypothesized to be due to the more hydroscopic nature of these LDBCs.

Glass transition temperature (T_g) decreased as a function of polyester type and hydrophobic mass ratio. LDBCs **90-L-G3** (57.7 °C) and **90-DL-G3** (52.3 °C) exhibit thermal features that are more representative of polylactide while that of **30-L-G3** (39.4 °C) and **30-DL-G3** (32.6 °C) correspond to that of PAMAM (Table S4). These results are reasonable as both LDBC sets are comprised of majority polylactide or PAMAM, respectively. Polymers **70-DL-G3** (39.4, 50.4 °C), **50-DL-G3** (36.5, 46.7 °C) and **70-L-G3** (41.2, 53.7 °C), **50-L-G3** (broaden ~39.6 °C) exhibited multiple T_gs. By comparing the thermograms in Figure 3, it appears that 70 and 50 % hydrophobic derivatives likely have similar volume between the hydrophilic and hydrophobic regions, resulting in contributions from both polymers being observable at the T_g.[46]

Self-Assembly and Morphology

Direct dissolution resulted in nanoparticles for LDBCs up to a 70-30 hydrophobic-hydrophilic mass ratio. Re-dispersion in water from the dry state was almost instantaneous, requiring little to no agitation. This observation is consistent with the variations in hydrophilic character of the PAMAM dendron used in previous studies[21] where the ionic nature of the terminal amines for **L-G3** and **DL-G3** (NH_3^+) increases

its hydrophilic character. When considering the potential future of our target materials and their pharmaceutical properties, this near instantaneous re-dispersion ability has both logistical and application advantages.

To understand the morphology of the self-assembled nanoparticles TEM analysis was conducted. Additionally, the TEM observations are further confirmed by SAXS analysis (*vide infra*). TEM captured aggregate morphologies of sizes (radii) ranging from 4.8 - 10.4 nm (Fig. 4 and enlarged images S25-30). Uranyl formate was used as a stain to increase the contrast between the hydrophilic and hydrophobic portions. LDBC **70-L-G3** shows a distribution of bilayered vesicles and elongated worm-like particles (Fig. 4a). **50-L-G3** produces bilayered vesicles with radii ranging from 4.8 - 6.1 nm (Fig. 4b). **30-L-G3** yields core-shell micelles with 7.1 nm radius (Fig. 4c). In comparison with **70-L-G3**, **70-DL-G3** showed bilayered vesicles, but no elongated worm like particles were observed (Fig. 4d). **50-DL-G3** (Fig. 4e) yields bilayered vesicles, and **30-DL-G3** (Fig. 4f) produces core-shell micelles with the radii of 6.0 nm, 5.3 nm respectively.

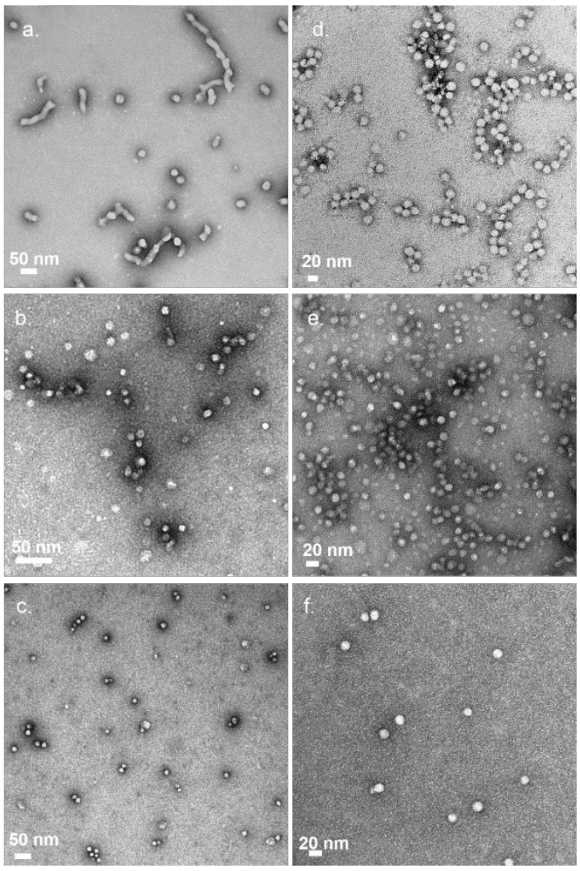

Figure 4. TEM images with utilizing uranyl formate as a contrast agent for (a) **70-L-G3**, (b) **50-L-G3**, (c) **30-L-G3**, (d) **70-DL-G3**, (e) **50-DL-G3** and (f) **30-DL-G3**; additional enlarged images are located in the ESI.

The formation of stable bilayered vesicles is an interesting achievement given the molecular weight of the PLA blocks are relatively short. Previously reported vesicles composed of block copolymers of PLA, e.g. PEG-PLLA required considerably higher molecular weights compared to our oligomeric sizes and hydrophobic weight ratios.[47]

Comparable hydrodynamic volumes were determined via DLS (Table S5, Fig. S19-S24) with zeta potentials ranging from +24.7 mV to +48.2 mV (Table S5) for nanoparticles prepared via direct dissolution. Such values of ±20-30 mV are viewed as highly stable and are common in drug delivery literature[48] as general guidelines classifying nanoparticle dispersions employ zeta potential data to correlate colloidal stability. The critical aggregate concentrations (CAC) for the LDBCs ranged from 0.91 to 9.75 mg/L (Table S6, Fig. S32-334) providing further evidence of stable nanoparticles.[49] The values are comparable to those found in literature and correlate to the candidacy of the copolymers as potential biomaterials. Specifically with the dependence of CAC on the length and weight ratio of PLA where an increase in hydrophobicity is shown to lead to a significant decrease in the CAC value.[50]

Concerning, however, are the high zeta potentials for nanoparticles formed from

50-L-G3 and **50-DL-G3.** There are conflicting reports regarding the ideal surface charge required for nanoparticle-assisted drug delivery.[51, 52] He et al. (cancer treatment) revealed that particles with less than 15 mV[53] surface charges exhibited ideal properties such as reduced macrophage uptake, longer circulation time and higher tumor retention.[54] However, it is well established that the charge effect of cell-uptake is cell type and surface charge dependent.[52, 55] For this study, the positively charged nanoparticles would penetrate into the cells more easily as the electronic potential of cell membranes are generally known to be negative.[52, 56] Nonetheless, high cytotoxicity due to the presence of extremely compact amino groups at the periphery of dendrimer structures like that of PAMAM have been well cited.[57, 58] Considering the size distribution and surface characteristics of nanoparticles in study, it should be noted that the surface properties of the nanostructures herein will not only determine the uptake efficiency of these materials but may also lead to severe drawbacks for future biological application.[59] Therefore, surface modification will be needed to minimize the positively charged surface comprised of PAMAM. Reducing the surface charge will aid to avoid any impending cytotoxic effects while maintaining their potential as carriers.

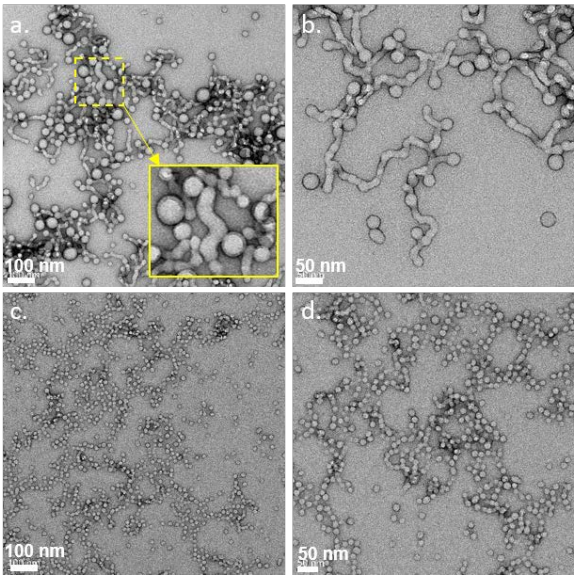

Figure 5.TEM images with utilizing uranyl formate as a contrast agent for (a and b) **90-L-G3**, (c and d) **90-DL-G3**. Nanoparticles were formed via conventional nanoprecipitation method as direct dissolution was not possible due to the high hydrophobic content.

By employing both stereochemical configurations of PLA, unique variations in thermal properties as well as morphology are expected. Any differences in morphology are a direct result of the varying stereoisomers of lactide (i.e. L vs DL) leading to diverse morphologies according to crystallinity and chain mobility.[60-62] Effects of the polyester type are apparent when comparing the CAC and hydrodynamic volumes for **L-G3** and **DL-G3** as the more amorphous PDLLA-PAMAM LDBCs tend to have smaller CAC values and radii (Tables S5-6).

However, these differences are minimal. The isomeric features of PLA are more evident for **90-L-G3** and **90-DL-G3**. LDBCs with >70 % PLA were prepared through

conventional nanoprecipitation method as direct dissolution in water was not possible due to the greater hydrophobic content. **90-L-G3** produces nanostructures which are kinetically "frozen" in intermediate (transition) states between worms, dumbbells and spheres (vesicles) (Fig. 5a-b). In the subset of Figure 5a, a snapshot of a spherical bud formation is observed in which a segment of a worm-like aggregate appears to separate off into a vesicle.[63] In contrast, **90-DL-G3** leads to the formation of predominately spherical nanostructures (vesicles), while transient structures are not observed (Fig 5c-d). When considering molecular thermodynamic effects, equilibration through chain-exchange is not likely due to the large interfacial tension between the PLA and water. Also, the nanoparticles were prepared at below the glass transition temperature of PLA (~52-54°C). Noack et al. have postulated the crystallization of the PLLA hydrophobic block following microphase separation in a selective solvent lead to destabilization of spherical particles which fuse with other spherical micelles to grow into worm-like aggregates.[64] In addition to the morphologies presented in Figures 4 and 5, elongated micelles, cubes, and tube-like nanostructures have been observed for these PLLA-PAMAM and PDLLA-PAMAM LDBCs under varying conditions. This work is currently on-going with efforts towards understanding the self-assembly mechanism using both computational modelling and analytical characterization.

SAXS Analysis

To study the morphology more in detail, SAXS experiments on the nanoparticles formed via direct dissolution were performed. An important goal in these studies was to determine bilayer thickness in our vesicles, especially with respect to LDBCs. The thickness of the vesicle wall strongly affects the size and stability of vesicles, and this thickness is primarily determined by the hydrophobic portion.[65-67] Polymer vesicles have also been shown to be able to adopt a multi-walled "onion" morphology with multiple alternating hydrophilic and hydrophobic regions.[68] This is unlikely to be observed by traditional microscopy methods and must be observed with SAXS (Fig.6, Table 2).

To describe SAXS data for micelles, we used a core-shell model[69, 70]

Table 2. Sample size direct from dissolution method: Radius of the core R_{core}, and the total radius $R_{totSAXS}$, radius of the macromolecule from TEM, R_{TEM}, hydrodynamic radius, R_{hDLS}, from DLS (intensity and number averaged distribution), and polydispersity, PD. All samples at volume fraction, ϕ = 0.1%.

LDBCs	SAXS model	$R_{coreSAXS}$ (nm)	$R_{totSAXS}$ (nm)	PD_{SAXS} (%)	R_{TEM} (nm)	PD_{TEM} (%)	R_{hDLS}[a] (nm)	PD_{DLS}[a] (%)
70-L-G3	core-shell vesicle	2.8±0.01	10.2±0.2	30	10.4±0.1	24±1	61.2±35, 25.3±3	48, 26
50-L-G3	core-shell vesicle	1.4±0.01	7.3±0.3	25	6.1±0.1	23±1	12.1±4, 9.5±1	28, 20
30-L-G3	core-shell micelle	0.8±0.01	7.2±0.1	20	7.1±0.1	30±2	7.8±1, 6.7±0.5	21, 28
70-DL-G3	core-shell vesicle	1.7±0.10	8.6±0.3 NA	21	9.6±0.1	21±1	10.5±3, 7.6±0.3	31, 22
50-DL-G3	core-shell vesicle	3.2±0.01	5.8±0.1	33	6.0±0.1	24±1	9.0±2, 5.8±1	30, 25
30-DL-G3	core-shell micelle	1.3± 0.01	7.4±0.2	18	5.3±0.1	22±1	9.0±2, 5.8±1	25, 25

[a] DLS reported in intensity and number averaged distribution

$$\frac{d\Sigma}{d\Omega}(Q) = \frac{\phi}{N_{agg}V_m}\left[I_{core}(Q) + I^{b}_{shell}(Q) + I_{inter}(Q) + I_{blob}(Q)\right] \quad (1)$$

Here, ϕ is the volume fraction, V_m is the total micellar volume of the block copolymer. For N_{agg}, defined as the aggregation number or the number of chains attached to the core, the terms $\mathrm{I_{core}(Q) = N_{agg}}^2\Delta\rho_{\mathrm{core}}{}^2 \cdot v_{\mathrm{core}}{}^2 \cdot \mathrm{A_{core}(Q)}^2$ correspond to the scattering from the core, with v_{core} as the volume of the core block copolymer (PLA block). The core contrast with respect to the solvent is given by their respective X-ray scattering length densities (XSLD) $\Delta\rho_{\mathrm{core}} = \rho_{\mathrm{core}} - \rho_{\mathrm{solvent}}$. $\mathrm{I^b_{shell}(Q) = N_{agg} \cdot (N_{agg} - B_{corr}) \cdot v_{shell}}{}^2 \cdot \Delta\rho_{\mathrm{shell}}{}^2 \cdot \mathrm{A_{shell}(Q)}^2$ describes the scattering from the corona (PAMAM block), with v_{shell}, the volume of the shell block copolymer and $\Delta\rho_{\mathrm{shell}} = \rho_{\mathrm{shell}} - \rho_{\mathrm{solvent}}$. The third term, $\mathrm{II_{inter}(Q) = 2\Delta\rho_{core} \cdot \Delta\rho_{shell} N_{agg}}{}^2 \cdot \mathrm{V_{core} \cdot V_{shell} \cdot A_{core}(Q) \cdot A_{shell}(Q)}$, is due to the interference between the core and the corona. The blob scattering from swollen corona is implemented following Svaneborg and Pedersen[71] as, $\mathrm{I_{blob}(Q) = V_{shell}}{}^2 \Delta\rho_{\mathrm{shell}}{}^2 \cdot \mathrm{P(Q)_{chain}}/(1 + \hat{\upsilon}\mathrm{P(Q)_{chain}})$. Here $A_{\mathrm{core}}(Q)$ and $A_{\mathrm{shell}}(Q)$, are the scattering amplitudes of the core (PLA) and shell (PAMAM) blocks, respectively. The interactions between the chains in the shell is given by the blob correlation parameter, $\mathrm{B_{corr} = 1/(1 + \hat{\upsilon})}$, where, $\hat{\upsilon}$, is an effective virial type parameter that scales with chain concentration in the shell.[71] The corresponding polydispersity index, *p*, for the micelles is calculated from the Gaussian distribution of the micellar corona, σ_m, which defines the relative width of the micellar surface at the micelle solvent interface. [69, 70]

In case of vesicles, the form factor is given by[72]

$$\frac{d\Sigma}{d\Omega}(Q) = \frac{\phi}{V_{shell}}\left[\frac{3V_{core}\Delta\rho_{shell}j_1(QR_{core})}{QR_{core}} + \frac{3V_{tot}\Delta\rho_{shell}j_1(QR_{tot})}{QR_{tot}}\right] \quad (2)$$

where V_{core}, V_{shell}, and V_{tot} are the core, shell and the total volumes, respectively. The shell thickness is given by $R_{\mathrm{tot}} - R_{\mathrm{core}}$, with R_{core}, the radius of the core and R_{tot}, the outer radius of the shell. Here the X-ray scattering length densities of the core and the solvent are identical whereas, j_1 is the spherical Bessel function, $j_1(QR_{\mathrm{tot}}) = (\sin(QR_{\mathrm{tot}}) - (QR_{\mathrm{tot}})\cos(QR_{\mathrm{tot}}))/(QR_{\mathrm{tot}})^2$. The polydispersity is modelled following the size distribution from TEM, which are compatible with Gaussian and log-normal distribution functions. [73]

Figure 6 represents the scattering intensity normalized by their volume fraction, ϕ. The data modelling was performed based on the TEM images. LDBCs **70-L-G3**, **50-L-G3**, **70-DL-G3**, and **50-L-G3**, the TEM images depict vesicle like spherical structures in Figure 5. The corresponding SAXS data was modelled using vesicle form factor as described in Equation 2. In case of **70-L-G3**, from TEM images although some wormlike arrangements of vesicles are observed, the spherical vesicle structure is statistically more dominant from the scattering measurements. The high Q scaling behavior

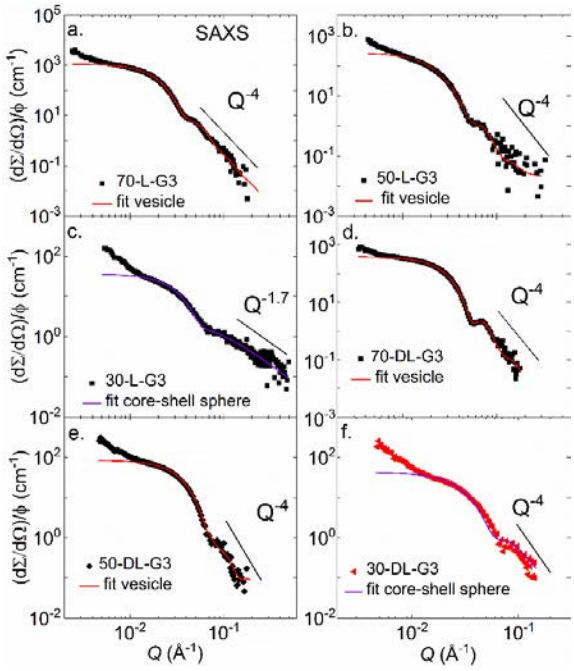

Figure 6. SAXS data for different PLA-PAMAM macromolecules normalized by their volume fraction ϕ. The data are modelled (solid lines) using core-shell sphere, core-shell cylinder (Equation 1) and vesicle form factors (Equation 2) as described in the text.

of ~ Q^{-4}, further supports the scattering from a smooth surface. LDBCs **30-DL-G3** and **30-L-G3** TEM images depicts spherical micellar structures. The shell thickness ($R_{tot} - R_{\mathrm{core}}$) for the vesicles in **70-L-G3** and **50-L-G3** and **DL-G3** systems represents the membrane thickness.

The corresponding SAXS data was also modelled using a micellar form factor described in Equation 1. As shown by the scattering intensity, ~ $Q^{-1.7}$, decay for real chains in good solvents,[74] is a characteristic feature of blob scattering from such micellar self-assemblies.[70, 75] The results from the SAXS data modelling are reported in Table 2. The increase in the scattering intensity at low-Q's indicates the onset of aggregates, which is verified by DLS. The sizes, $R_{\_totSAXS}$ and, $R_{\_TEM}$, from SAXS, and TEM in Table 2 are identical within the experimental uncertainties, whereas, $R_{\_hDLS}$ from DLS depends on the intensity and number averaged distribution. The discrepancy with the results from DLS is attributed to the high polydispersity for **70-L-G3** in which various aggregates were observed yet accurate determination of the dimension of the cylinder from SAXS and TEM was still achieved.

CONCLUSIONS

In this work, we have developed a feasible synthetic strategy to afford LDBCs that are composed of PAMAM and PLA. These materials are made with a high percent conversion (83 % - 94 %) indicating an ease in the synthetic route taken for a series of copolymers capable of self-assembly at varying hydrophobic ratios. By only modifying the degree of polymerization of the hydrophobic portion, we were able to obtain multiple morphologies and sizes from the same reaction mechanism. Direct dissolution provides a facile and biocompatible methodology of nanoparticle preparation for these copolymers, resulting in nanoparticles bearing positive surface charges. Thermal analysis shows that the behavior of these LDBCs represent combination of both polymeric segments. The details of the morphology were elucidated by TEM and SAXS, confirming these polymers exhibited selective self-assembly into the desired morphology of vesicles and core-shell micelles.

Advancing this study towards therapeutic drug delivery, reducing the surface charge will be done to avoid impending cytotoxic effects while maintaining the potential of the nanostructure as carriers. Within this scope, bilayer vesicles will be of particular interest due to their biomimetic nature which provides increased biocompatibility, while also serving as a dual-purpose drug carrier

for the simultaneous delivery of both hydrophobic and/or hydrophilic drugs.[76]

In summary, the current work provides a suitable foundation for understanding how the chemical make-up of the LDBC affects the overall self-assembled structure. Ongoing research is aimed towards the assembly of interest, surface modification and exploitation of beneficial structural properties for future applications.

ACKNOWLEDGEMENTS

I.C., D.G.A., J.S.D.W., W.D.R., B.L.S., D.L.W. appreciates financial support of this work from the University of Mississippi. This work made use of the BioCryo facility of Northwestern University's NUANCE Center, which has received support from the Soft and Hybrid Nanotechnology Experimental (SHyNE) Resource (NSF ECCS-1542205); the MRSEC program (NSF DMR-1720139) at the Materials Research Center; the International Institute for Nanotechnology (IIN); and the State of Illinois, through the IIN. It also made use of the CryoCluster equipment, which has received support from the MRI program (NSF DMR-1229693). The work also made use of the Material Research Laboratory (MRL) Shared Experimental Facilities at University of California at Santa Barbara. The MRL Shared Experimental Facilities are supported by the MRSEC Program of the NSF under Award No. DMR 1720256; a member of the NSF-funded Materials Research Facilities Network (www.mrfn.org). This research used resources of the Advanced Photon Source, a U.S. Department of Energy (DOE) Office of Science User Facility operated for the DOE Office of Science by Argonne National Laboratory under Contract No. DE-AC02-06CH11357. The X-ray scattering work is supported by the U.S. Department of Energy (DOE) under EPSCoR Grant No. DE-SC0012432 with additional support from the Louisiana Board of Regents. M.E.P. was supported by the LA Board of Regents graduate fellowship. MALDI was supported by NSF (MRI-0619770) and the GPC by Louisiana Board of Regents (25MUL-15)

REFERENCES AND NOTES

1. A.-M. Caminade and C.-O. Turrin, *Journal of Materials Chemistry B*, 2014, **2**, 4055-4066.
2. E. R. Gillies and J. M. J. Fréchet, *Drug Discovery Today*, 2005, **10**, 35-43.
3. M. L. Adams, A. Lavasanifar and G. S. Kwon, *Journal of Pharmaceutical Sciences*, 2003, **92**, 1343-1355.
4. F. Wurm and H. Frey, *Progress in Polymer Science*, 2011, **36**, 1-52.
5. I. Gitsov, K. L. Wooley, C. J. Hawker, P. T. Ivanova and J. M. J. Frechet, *Macromolecules*, 1993, **26**, 5621-5627.
6. B. N. S. Thota, L. H. Urner and R. Haag, *Chemical Reviews*, 2016, **116**, 2079-2102.
7. V. Percec, D. A. Wilson, P. Leowanawat, C. J. Wilson, A. D. Hughes, M. S. Kaucher, D. A. Hammer, D. H. Levine, A. J. Kim, F. S. Bates, K. P. Davis, T. P. Lodge, M. L. Klein, R. H. DeVane, E. Aqad, B. M. Rosen, A. O. Argintaru, M. J. Sienkowska, K. Rissanen, S. Nummelin and J. Ropponen, *Science*, 2010, **328**, 1009-1014.
8. J. M. J. Fréchet, *Proceedings of the National Academy of Sciences*, 2002, **99**, 4782-4787.
9. A.-M. Caminade, R. Laurent, B. Delavaux-Nicot and J.-P. Majoral, *New Journal of Chemistry*, 2012, **36**, 217-226.
10. Q. Xiao, J. D. Rubien, Z. Wang, E. H. Reed, D. A. Hammer, D. Sahoo, P. A. Heiney, S. S. Yadavalli, M. Goulian, S. E. Wilner, T. Baumgart, S. A. Vinogradov,

M. L. Klein and V. Percec, *Journal of the American Chemical Society*, 2016, **138**, 12655-12663.
11. M. Labieniec-Watala and C. Watala, *Journal of Pharmaceutical Sciences*, 2015, **104**, 2-14.
12. R. M. Kannan, E. Nance, S. Kannan and D. A. Tomalia, *Journal of Internal Medicine*, 2014, **276**, 579-617.
13. D. Lombardo, P. Calandra, D. Barreca, S. Magazu and M. A. Kiselev, *Nanomaterials (Basel, Switzerland)*, 2016, **6**.
14. S. E. A. Gratton, P. A. Ropp, P. D. Pohlhaus, J. C. Luft, V. J. Madden, M. E. Napier and J. M. DeSimone, *Proceedings of the National Academy of Sciences*, 2008, **105**, 11613-11618.
15. R. Esfand and D. A. Tomalia, *Drug Discovery Today*, 2001, **6**, 427-436.
16. D. Garlotta, *Journal of polymers and the environment*, 2001, **v. 9**, pp. 63-84-2001 v.2009 no.2002.
17. K. E. Uhrich, S. M. Cannizzaro, R. S. Langer and K. M. Shakesheff, *Chemical Reviews*, 1999, **99**, 3181-3198.
18. Q. Cai, Y. Zhao, J. Bei, F. Xi and S. Wang, *Biomacromolecules*, 2003, **4**, 828-834.
19. C. Hua, S.-M. Peng and C.-M. Dong, *Macromolecules*, 2008, **41**, 6686-6695.
20. W. Cao and L. Zhu, *Macromolecules*, 2011, **44**, 1500-1512.
21. H. Qiao, J. Li, Y. Wang, Q. Ping, G. Wang and X. Gu, *International journal of pharmaceutics*, 2013, **452**, 363-373.
22. I. Gitsov, P. T. Ivanova and J. M. J. Fréchet, *Macromolecular Rapid Communications*, 1994, **15**, 387-393.
23. C. Booth, J. L. Forget, I. Georgii, W. S. Li and C. Price, *European Polymer Journal*, 1980, **16**, 255-259.
24. H. He, M. Zhong, B. Adzima, D. Luebke, H. Nulwala and K. Matyjaszewski, *Journal of the American Chemical Society*, 2013, **135**, 4227-4230.
25. N. D. Hann, *Journal of Polymer Science: Polymer Chemistry Edition*, 1977, **15**, 1331-1339.
26. G.-Y. Liu, C.-J. Chen and J. Ji, *Soft Matter*, 2012, **8**, 8811-8821.
27. S. Rangelov and A. Pispas, *Polymer and polymer-hybrid nanoparticles: from synthesis to biomedical applications*, CRC Press, 2013.
28. S. McRae Page, M. Martorella, S. Parelkar, I. Kosif and T. Emrick, *Molecular Pharmaceutics*, 2013, **10**, 2684-2692.
29. C. J. Martínez Rivas, M. Tarhini, W. Badri, K. Miladi, H. Greige-Gerges, Q. A. Nazari, S. A. Galindo Rodríguez, R. Á. Román, H. Fessi and A. Elaissari, *International journal of pharmaceutics*, 2017, **532**, 66-81.
30. J. Ilavsky, *Journal of Applied Crystallography*, 2012, **45**, 324-328.
31. J.-C. Buffet and J. Okuda, *Polymer Chemistry*, 2011, **2**, 2758-2763.
32. J. Bugno, H. J. Hsu and S. Hong, *Journal of drug targeting*, 2015, **23**, 642-650.
33. H. R. Kricheldorf, *Polymers for Advanced Technologies*, 2002, **13**, 969-974.
34. B. G. G. Lohmeijer, R. C. Pratt, F. Leibfarth, J. W. Logan, D. A. Long, A. P. Dove, F. Nederberg, J. Choi, C. Wade, R. M. Waymouth and J. L. Hedrick, *Macromolecules*, 2006, **39**, 8574-8583.
35. F. Nederberg, E. F. Connor, M. Möller, T. Glauser and J. L. Hedrick, *Angewandte Chemie International Edition*, 2001, **40**, 2712-2715.

36. N. E. Kamber, W. Jeong, R. M. Waymouth, R. C. Pratt, B. G. G. Lohmeijer and J. L. Hedrick, *Chemical Reviews*, 2007, **107**, 5813-5840.
37. A. P. Dove, *ACS Macro Letters*, 2012, **1**, 1409-1412.
38. M. H. Chisholm, *Pure and Applied Chemistry*, 2010, **82**, 1647-1662.
39. D. G. Abebe, R. Kandil, T. Kraus, M. Elsayed, O. M. Merkel and T. Fujiwara, *Macromolecular Bioscience*, 2015, **15**, 698-711.
40. E. B. Yalcin and S. M. de la Monte, *The journal of histochemistry and cytochemistry : official journal of the Histochemistry Society*, 2015, **63**, 762-771.
41. R. Giordanengo, S. Viel, M. Hidalgo, B. Allard-Breton, A. Thévand and L. Charles, *Journal of the American Society for Mass Spectrometry*, 2010, **21**, 1075-1085.
42. in *Monitoring Polymerization Reactions*, DOI: doi:10.1002/9781118733813.ch5.
43. in *Monitoring Polymerization Reactions*, DOI: doi:10.1002/9781118733813.ch10.
44. B. D. Ulery, L. S. Nair and C. T. Laurencin, *Journal of Polymer Science Part B: Polymer Physics*, 2011, **49**, 832-864.
45. K. Madhavan Nampoothiri, N. R. Nair and R. P. John, *Bioresource technology*, 2010, **101**, 8493-8501.
46. S. Strandman and X. X. Zhu, *Progress in Polymer Science*, 2015, **42**, 154-176.
47. Z. Wang, Y. Cao, J. Song, Z. Xie and Y. Wang, *Langmuir*, 2016, **32**, 9633-9639.
48. S. Bhattacharjee, *Journal of controlled release : official journal of the Controlled Release Society*, 2016, **235**, 337-351.
49. S. C. Owen, D. P. Y. Chan and M. S. Shoichet, *Nano Today*, 2012, **7**, 53-65.
50. H. Yin, S.-W. Kang and Y. H. Bae, *Macromolecules*, 2009, **42**, 7456-7464.
51. S. M. Sadat, S. T. Jahan and A. Haddadi, *Journal of Biomaterials and Nanobiotechnology*, 2016, **7**, 91.
52. E. Fröhlich, *International journal of nanomedicine*, 2012, **7**, 5577-5591.
53. C. He, Y. Hu, L. Yin, C. Tang and C. Yin, *Biomaterials*, 2010, **31**, 3657-3666.
54. F. S. Mozar and E. H. Chowdhury, *Current pharmaceutical design*, 2018, **24**, 3283-3296.
55. T.-H. Chung, S.-H. Wu, M. Yao, C.-W. Lu, Y.-S. Lin, Y. Hung, C.-Y. Mou, Y.-C. Chen and D.-M. Huang, *Biomaterials*, 2007, **28**, 2959-2966.
56. X. R. Shao, X. Q. Wei, X. Song, L. Y. Hao, X. X. Cai, Z. R. Zhang, Q. Peng and Y. F. Lin, *Cell proliferation*, 2015, **48**, 465-474.
57. B. H. Zinselmeyer, S. P. Mackay, A. G. Schatzlein and I. F. Uchegbu, *Pharmaceutical research*, 2002, **19**, 960-967.
58. D. Luong, P. Kesharwani, R. Deshmukh, M. C. I. Mohd Amin, U. Gupta, K. Greish and A. K. Iyer, *Acta Biomaterialia*, 2016, **43**, 14-29.
59. L. Hu, Z. Mao and C. Gao, *Journal of Materials Chemistry*, 2009, **19**, 3108-3115.
60. A. Halperin, M. Tirrell and T. P. Lodge, in *Macromolecules: Synthesis, Order and Advanced Properties*, Springer Berlin Heidelberg, Berlin, Heidelberg, 1992, DOI: 10.1007/BFb0051635, pp. 31-71.
61. B. K. Johnson and R. K. Prud'homme, *Physical Review Letters*, 2003, **91**, 118302.

62. H. Cui, Z. Chen, S. Zhong, K. L. Wooley and D. J. Pochan, *Science*, 2007, **317**, 647-650.
63. R. Lund, L. Willner, D. Richter and E. E. Dormidontova, *Macromolecules*, 2006, **39**, 4566-4575.
64. S. Noack, D. Schanzenbach, J. Koetz and H. Schlaad, *Macromolecular Rapid Communications*, 2019, **40**, 1800639.
65. W. Rawicz, K. C. Olbrich, T. McIntosh, D. Needham and E. Evans, *Biophysical Journal*, 2000, **79**, 328-339.
66. M. Kranenburg, M. Vlaar and B. Smit, *Biophysical journal*, 2004, **87**, 1596-1605.
67. M. Peterca, V. Percec, P. Leowanawat and A. Bertin, *Journal of the American Chemical Society*, 2011, **133**, 20507-20520.
68. S. Zhang, H.-J. Sun, A. D. Hughes, R.-O. Moussodia, A. Bertin, Y. Chen, D. J. Pochan, P. A. Heiney, M. L. Klein and V. Percec, *Proceedings of the National Academy of Sciences*, 2014, **111**, 9058-9063.
69. S. Gupta, M. Camargo, J. Stellbrink, J. Allgaier, A. Radulescu, P. Lindner, E. Zaccarelli, C. N. Likos and D. Richter, *Nanoscale*, 2015, **7**, 13924-13934.
70. R. Lund, V. Pipich, L. Willner, A. Radulescu, J. Colmenero and D. Richter, *Soft Matter*, 2011, **7**, 1491-1500.
71. J. S. Pedersen, C. Svaneborg, K. Almdal, I. W. Hamley and R. N. Young, *Macromolecules*, 2003, **36**, 416-433.
72. J. Pencer and F. R. Hallett, *Langmuir*, 2003, **19**, 7488-7497.
73. G. Walter, R. Kranold, T. Gerber, J. Baldrian and M. Steinhart, *Journal of Applied Crystallography*, 1985, **18**, 205-213.
74. P.-G. De Gennes and P.-G. Gennes, *Scaling concepts in polymer physics*, Cornell university press, 1979.
75. S. Gupta, M. Camargo, J. Stellbrink, J. Allgaier, A. Radulescu, P. Lindner, E. Zaccarelli, C. N. Likos and D. Richter, *Nanoscale*, 2015, **7**, 13924-13934.
76. E. Blanco, H. Shen and M. Ferrari, *Nature Biotechnology*, 2015, **33**, 941.

GRAPHICAL ABSTRACT

Indika Chandrasiri,[a] Daniel G. Abebe,[a] Sudipta Gupta,[b] Jon Steven Dal Williams,[a] William D. Rieger,[a] Briana L. Simms,[a] Mahesh Loku Yaddehige,[a] YeRim Noh,[b] Molly E. Payne,[d] Alexander W. Fortenberry,[c] Adam E. Smith,[c] Jan Ilavsky, [e] Scott M. Grayson, [d] Gerald J. Schneider[b,f] and Davita L. Watkins[a*]

Synthesis and Characterization of Polylactide-PAMAM "Janus-type" Linear-Dendritic Hybrids

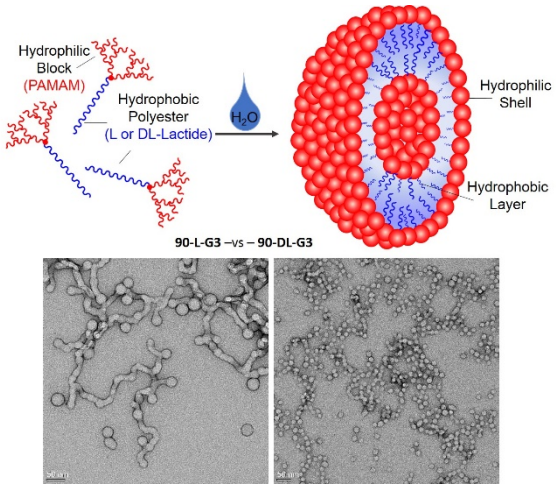

A library of polyester-PAMAM (i.e., polyester: polylactide, PLA (hydrophobic) and polyamidoamine, PAMAM (hydrophilic)) polymers were synthesized and their resulting nanoparticles were studied. The synthetic methodology afforded a wide-range of LDBCs compositions with up to 90 weight % hydrophobic content—all of which were capable of self-assembling into stable nanostructures in aqueous solution. By employing both stereochemical configurations of PLA, distinct thermal properties as well as morphology were observed.